ACS APPLIED MATERIALS & INTERFACES

www.acsami.org

Research Article

Self-Compensating Liquid-Repellent Surfaces with Stratified Morphology

Songtao Hu, Xiaobao Cao, Tom Reddyhoff, Debashis Puhan, Sorin-Cristian Vladescu, Qian Wang, Xi Shi,* Zhike Peng,* Andrew J. deMello, and Daniele Dini

Cite This: *ACS Appl. Mater. Interfaces* 2020, 12, 4174–4182

Read Online

ACCESS | Metrics & More | Article Recommendations | Supporting Information

ABSTRACT: Artificial liquid-repellent surfaces have recently attracted vast scientific attention; however, achieving mechanical robustness remains a formidable challenge before industrialization can be realized. To this end, inspired by plateaus in geological landscapes, a self-compensating strategy is developed to pave the way for the synthesis of durable repellent surfaces. This self-compensating surface comprises tall hydrophobic structural elements, which can repel liquid droplets. When these elements are damaged, they expose shorter structural elements that also suspend the droplets and thus preserve interfacial repellency. An example of this plateau-inspired stratified surface was created by three-dimensional (3D) direct laser lithography micro−nano fabrication. Even after being subjected to serious frictional damage, it maintained static repellency to water with a contact angle above 147° and was simultaneously able to endure high pressures arising from droplet impacts. Extending the scope of nature-inspired functional surfaces from conventional biomimetics to geological landscapes, this work demonstrates that the plateau-inspired self-compensating strategy can provide an unprecedented level of robustness in terms of sustained liquid repellency.

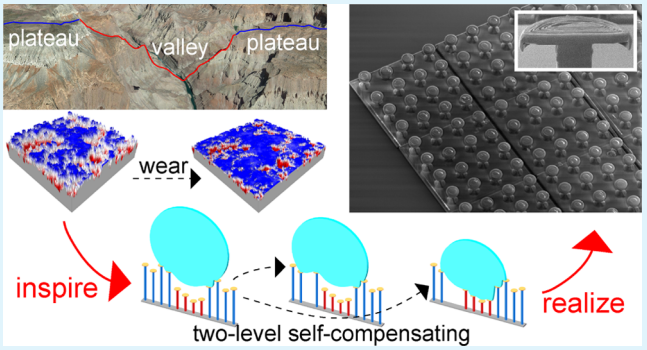

KEYWORDS: *artificial surface, 3D laser lithography, liquid repellency, mechanical robustness, friction*

1. INTRODUCTION

Natural surfaces, serving as the interface between an organism and its surroundings, have to fulfill inherent functions responding to environmental physicochemical reactions by optimizing the morphological structure and chemical composition. As a common pathway in biomimetics, understanding and mimicking morphological and chemical attributes from biological evolution provides an ideal strategy to translate fascinating functions of natural surfaces into synthetic systems.[1] One interesting natural inspiration is the liquid-repellent nature of surfaces, which has attracted great attention because of its scientific and economic importance in applications of self-cleaning,[2] antifogging,[3] anti-icing,[4] antireflection,[5] water harvesting,[6] bio-analysis,[7] microdroplet manipulation,[8] etc. The most well-known example is the lotus effect that exhibits water repellency by combining hierarchical morphology and wax-based chemical decoration,[9] with the former serving as the crucial factor. However, hierarchical surfaces, even if embellished by chemical modification of low-surface-energy materials, still encounter limitations that prevent mature industrialization. For instance, most repellency is effective for aqueous liquids but fails for low-surface-tension liquids such as oils and organic solvents; moreover, repellency is usually restricted to static conditions relating to droplet condensation at high relative humidity and is limited in kinetic circumstances associated with high-velocity impacting events such as rain droplets. Excitingly, springtails, the most widespread arthropods on Earth,[10] present a mushroom-like geometry on their cuticles that has evolved to avoid wetting by water and organic liquids so as to guarantee dermal respiration in aqueous habitats and temporarily flooded environments. This mushroom-like topology has contributed to the ideation of a competitive design employing singly/doubly/triply re-entrant head structures atop supporting pillars,[11−19] overcoming the aforementioned limitations even regardless of chemical modification.

Mechanical robustness is a major challenge in designing and processing artificial repellent surfaces and is regarded as limiting the uptake of pillar-based surfaces in commercial applications.[10] Interfacial repellency usually diminishes after a period of time due to breakages occurring at the base and the nick under a shear load. In general, hard materials such as metals and ceramics seem to be a solution to improve structural durability; however, they

Received: December 18, 2019
Accepted: December 31, 2019
Published: December 31, 2019

https://dx.doi.org/10.1021/acsami.9b22896
ACS Appl. Mater. Interfaces 2020, 12, 4174–4182

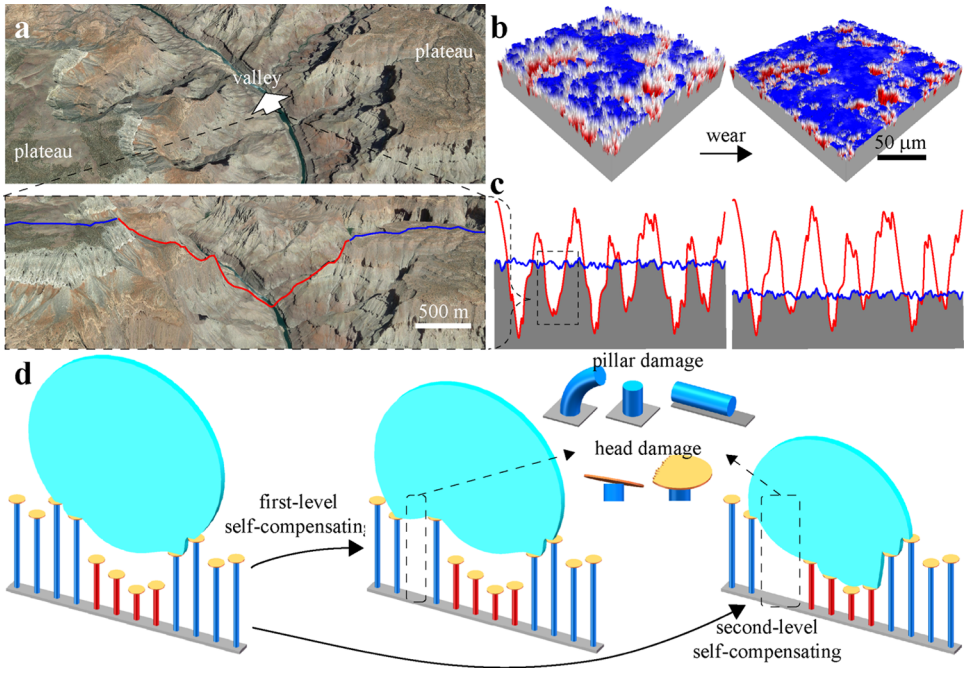

Figure 1. Ideation of self-compensating liquid-repellent surface. (a) Bi-Gaussian stratified morphology of plateaus observed in the Grand Canyon National Park from top and side views. (b) Bi-Gaussian stratified morphology observed on engineering surfaces before/after frictional wear. (c) 2D schematic diagram of a bi-Gaussian stratified morphology to ensure a stable and sustained wear resistance. (d) Schematic diagram of a self-compensating surface with underlying pillars following a bi-Gaussian stratified height distribution to prolong the liquid repellency of mushroom−pillar structures.

can trigger an even worse resistance than soft materials owing to the loss of compliance. Thus, self-supporting networks have been added to interconnect adjacent underlying structures so as to enhance the mechanical stability in comparison to an array of individual supporting structures.[15] To recover repellency that would otherwise be reduced by these additive self-supporting networks, the fabrication of an undulated substrate is strongly recommended.[18] Another approach elaborated to improve interfacial durability is the self-healing concept, whereby preserving agents encapsulated in structural pores can quickly migrate into the damaged regions.[20,21] For this self-healing strategy, more studies are further required by interfacial structures under a regular pattern in comparison to the existing scenario with the structures following a random distribution.

Here, we report a peculiar artificial surface inspired by bi-Gaussian stratified plateaus existing in natural landscapes and engineering industries, whose realization and response are shown to provide a promising morphological, self-compensation strategy to improve interfacial durability (see Figure 1). Unlike the aforementioned self-supporting and self-healing strategies, the short structural elements on our surface will automatically inherit the repelling roles played by the taller ones when the latter are damaged due to mechanical contact and friction, thereby ensuring stable and sustained liquid repellency. Using three-dimensional (3D) direct laser lithography micro−nano fabrication, we have realized our plateau-inspired self-compensating design and have demonstrated its water repellency in both static and kinetic circumstances following mechanical damage induced by sliding friction.

2. EXPERIMENTAL SECTION

2.1. Surface Modeling. The simulation method of bi-Gaussian stratified morphology (see Section S1) was implemented in Matlab (Mathworks Inc.) to generate the pillar−height matrix according to the prescribed bi-Gaussian stratified indexes (see Table S1). Mushroom−pillar structures were modeled in SolidWorks (Dassault Systemes, France) whose heights were set as the above matrix. The resulting 3D model of the plateau-inspired surface was output at a stereolithography format. This approach was also adopted to model the other four plateau-inspired surfaces with emulated mechanical damage.

2.2. Surface Fabrication. On Photonic Professional System (NanoScribe GmbH, Germany), the IP-S photoresist (NanoScribe GmbH, Germany) was exposed to a 780-nm femtosecond laser through an oil-immersion objective at a speed of 100 mm·s^{-1} with a power of 110 mW so as to be fabricated on an indium tin oxide (ITO)-coated fused silica. The laser was commanded to write 0.5 μm beneath the interface between the photoresist and the substrate, thus ensuring a strong adhesion between the printed structures and the glass substrate. The fabrication was then developed for 20 min in SU-8 Developer (MicroChem Corp.) and rinsed in isopropyl alcohol and deionized water.

2.3. Morphology Characterization. The morphologies of fabricated surfaces were inspected by MXB-2500REZ (Hirox Europe Ltd., France) and S-3400N SEM (Hitachi Ltd., Japan) accounting for a multiscale requirement.

2.4. Contact Angle Measurement. The contact angle of water droplets (4 μL) was measured on a Rame−Hart Contact Angle Goniometer (Rame-Hart Instrument Co.) in a sessile drop mode under controlled temperature (20 °C) and relative humidity (45%). Each contact angle was captured 30 s after the droplet contacted the fabricated surface so as to ensure equilibrium. Also, a water droplet (4 μL) was created and held by the syringe above the fabricated surface so as to measure the contact angle hysteresis through capturing the advancing and receding angles by sliding the positioning platform at a velocity of 100 μm·s^{-1}.[14] The measurement was conducted five times on the same fabricated surface for repeatability.

2.5. Droplet Impacting Test. The spreading, retracting, and after-retracting behaviors after water droplets impacted the fabricated surface were captured by Phantom Miro ex2 (AMETEK Inc.) assembled with Zoom 7000 (Navitar Inc.) with a sampling rate of 2900 fps. A microsyringe pump was used to release water droplets with a volume of

https://dx.doi.org/10.1021/acsami.9b22896
ACS Appl. Mater. Interfaces 2020, 12, 4174−4182

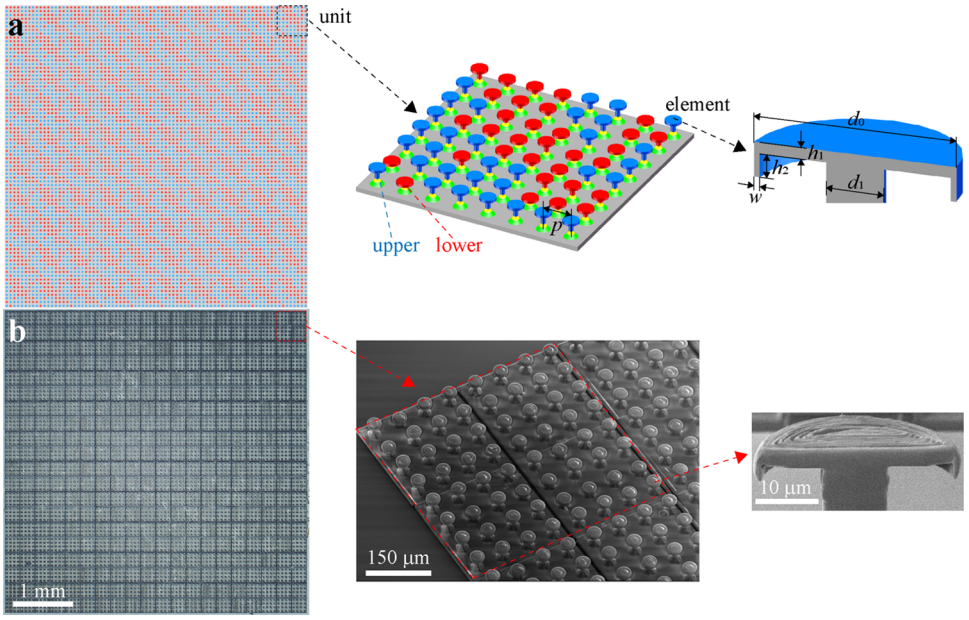

Figure 2. Self-compensating liquid-repellent surface. (a) Design of a self-compensating surface as a matrix consisting of 10 × 10 units, each unit encompassing 8 × 8 mushroom−pillar elements following a bi-Gaussian stratified height distribution. (b) Fabrication of the self-compensating surface.

4 μL. The height to release the droplets was changed to realize the adjustment of *We*.

2.6. Friction Test. The friction test was conducted by loading and sliding a triangular rubber wiper against the printed surface on CETR UMT (Bruker Corp.). This equipment was operated in a pin-on-disc mode so that the printed surface was held stationary as the lower specimen, while the wiper had a controlled movement as the upper specimen. The wiper was declined to generate a line contact with the printed surface near one edge at a normal load of 0.2 N and then was slid over the surface at a speed of 1 mm·s^{-1} at an unchanged normal distance. The normal and frictional loads were recorded at a step of 5 ms. After the friction test, the printed surface was rinsed in isopropyl alcohol and deionized water.

3. RESULTS AND DISCUSSION

3.1. Ideation of Self-Compensating Design. To achieve stable and sustained repellency, we designed an artificial self-compensating surface with its structural elements composed of mushroom heads atop pillars following a bi-Gaussian stratified height distribution, inspired by plateau morphologies existing in geological landscapes (see Figure 1a) and engineering industries (see Figure 1b). Similar to the fractal concept motivated by natural landscapes (e.g., coastlines), a bi-Gaussian stratified morphology can be clearly observed on plateaus such as in the Grand Canyon National Park, where the initial mountains generated in past diastrophisms have been truncated by environmental actions of wind and rain so as to engender flat plateaus interpenetrated by deep valleys. In fact, this peculiar morphology can also be found on engineering surfaces subjected to frictional wear,[22,23] and has been modeled to a large-scale roughness (see the red lower component in Figure 1c) intersected by a small-scale roughness (see the blue upper component), with each component individually respecting a Gaussian height distribution due to the randomness of a wear process. Notably, as opposed to the classical fractal characteristic emphasizing the self-similarity at different scales, the bi-Gaussian one renders its stratified property (i.e., retaining the lower height in the combination of the upper and lower components) at a single scale.

Researchers have long overlooked the real-life bi-Gaussian stratified nature of surfaces because of its simplification to a single-stratum, non-Gaussian modeling (e.g., exponential). However, the bi-Gaussian stratified characteristic, recently, has captivated scientists and engineers for its impressive functions arising from its particular stratified topology in comparison to a uniform height or a Gaussian distribution in terms of friction[22,23] and wettability.[24,25] Looking at the frictional field, as the upper component plays critical roles in load-bearing and wear resistance while the lower component serves as lubricant reservoirs and debris traps, the performance of an engineering surface can be manually designed by controlling the configuration of the two components.[22] Specifically, the upper component of an unused engineering surface is designed to individually resist the opponent body at the start of the service; then, along with the frictional wear, the mean height of the upper component declines gradually relative to the lower component, making more and more surface nodes transform into the upper component (see Figure 1b,c) so as to gain a stable and sustained wear resistance.[23] Accordingly, this noteworthy attribute of a bi-Gaussian stratified morphology triggers a window of opportunity for a self-compensating strategy to improve the durability of springtail-inspired repellent surfaces (see Figure 1d). More precisely, all mushroom−pillar elements on an artificial surface can be divided into two layers in terms of element heights, where the upper-layer elements are well designed to guarantee liquid repellency; with the repellent loss of an upper-layer element induced by mechanical damage under a slight shear load, other upper-layer elements will be exposed to grab the role of the broken one (termed as the first-level self-compensating); when most upper-layer elements lose their repellency under a heavy shear load, some elements on the lower layer will be activated (termed as the second-level self-compensating). As opposed to mechanically robust surfaces by use of a hierarchical design based on a multiscale, fractal characteristic,[26] the single-scale, stratified property of our bi-Gaussian characteristic provides a pure microscale solution to improve the mechanical robustness of liquid-repellent surfaces.

https://dx.doi.org/10.1021/acsami.9b22896
ACS Appl. Mater. Interfaces 2020, 12, 4174−4182

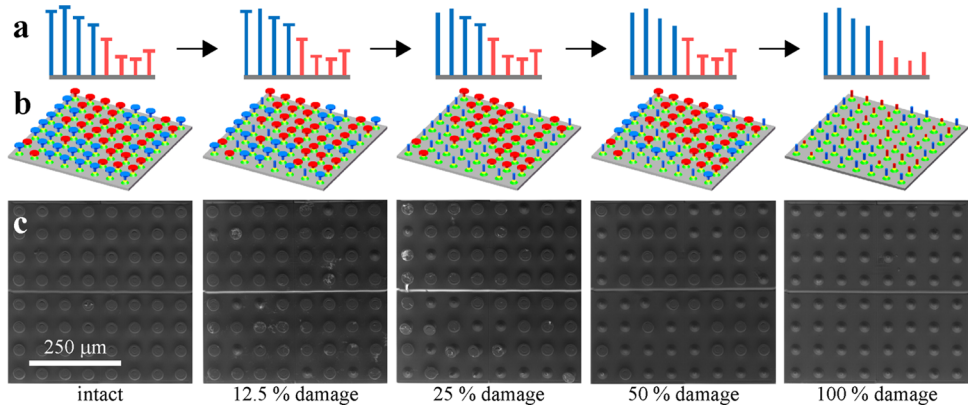

Figure 3. Self-compensating liquid repellent surface in an emulated evolution of mechanical damage. (a) Schematic diagram of an emulated evolution of mechanical damage due to contact and friction, where a mushroom-head disappearance propagated from high to low: intact, 12.5% damage, 25% damage, 50% damage, and complete damage. (b, c) Unit design and fabrication of the self-compensating surface with emulated mechanical damage, where fabrication images were captured after static and kinetic repellent experiments, indicating an excellent structural strength.

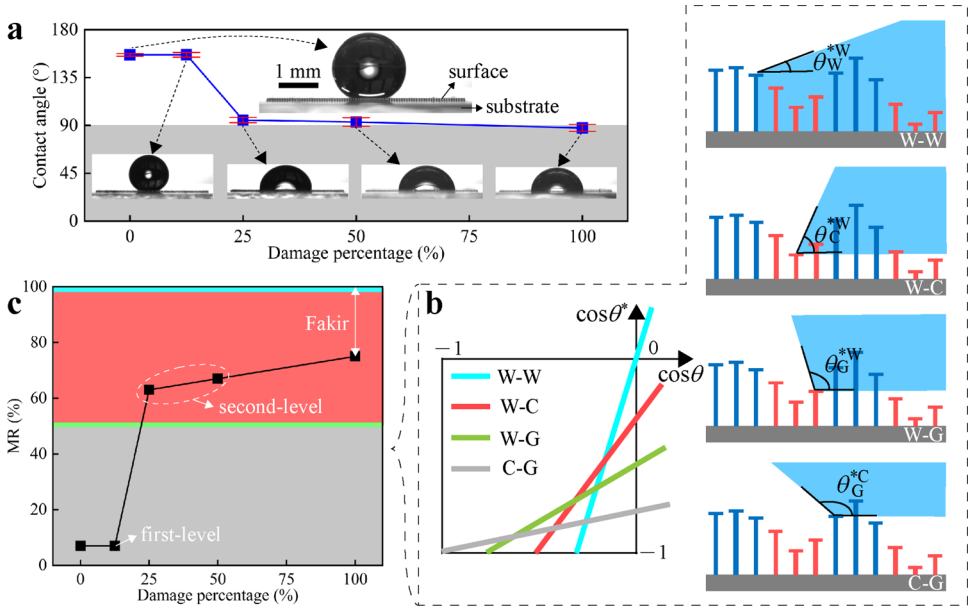

Figure 4. Static water repellency of the self-compensating surface with emulated mechanical damage. (a) Contact angles of water droplets. (b, c) Wetting states of the upper and lower layers by using a bi-Gaussian stratified wetting model consisting of four wetting substates, i.e., W−W, W−C, W−G, and C−G.

3.2. Design and Fabrication of a Self-Compensating Surface. A self-compensating surface (see Figure 2a) was purposely designed as a 5 × 5 mm^2 matrix consisting of 10 × 10 units, each unit encompassing 8 × 8 elements with mushroom heads atop pillars (namely, element distance p equals to 62.5 μm). The reason for such a matrix design was related to the scientific demand for eliminating the repetitive error caused by different contacting positions in the following static and kinetic repellent experiments. For each element, a doubly re-entrant head was utilized by setting d_0 to 35 μm, h_1 to 2 μm, h_2 to 4 μm, and w to 1 μm. Meanwhile, the heights of underlying pillars (d_1 = 10 μm) in each unit were designed to follow a bi-Gaussian stratified distribution, thus yielding an obvious two-layer arrangement. The pillar heights were prescribed by bi-Gaussian stratified indexes (defined in Figure S1) including the root-mean-square height of upper-layer pillars *Spq*, the root-mean-square height of lower-layer pillars *Svq*, and the proportion of upper-layer pillars *Smq*. In addition, an extra reinforced structure was introduced to strengthen the mechanical property at the pillar bottom as well as to intensify the adhesion between the pillar bottom and the substrate. Also, a fillet was employed accounting for a smooth transition between the reinforcement and the pillar to eliminate the shear load arising from an abrupt shape change.

The designed surface was realized with 3D direct laser lithography on a Photonic Professional System (NanoScribe GmbH, Germany) by fabricating the target structures made of IP-S photoresist (NanoScribe GmbH, Germany) on an ITO-coated fused silica via a two-photon polymerization (see Figure 2b). Notably, the NanoScribe system can be regarded as the most precise rapid prototyping technology to tailor 3D structures at a micrometric level even at nanoscale. This up-to-date technology has been successfully applied in optics,[27] photonics,[28] microfluidic,[29] biology,[30] mechanical metamaterials,[31] etc., and has recently paved the way to shed light on the wetting mechanism.[6,19,25,32−34] Thanks to the optimization of structural design and processing technic (see Figure S2), artificial mushroom−pillar structures were strongly attached to

https://dx.doi.org/10.1021/acsami.9b22896
ACS Appl. Mater. Interfaces 2020, 12, 4174−4182

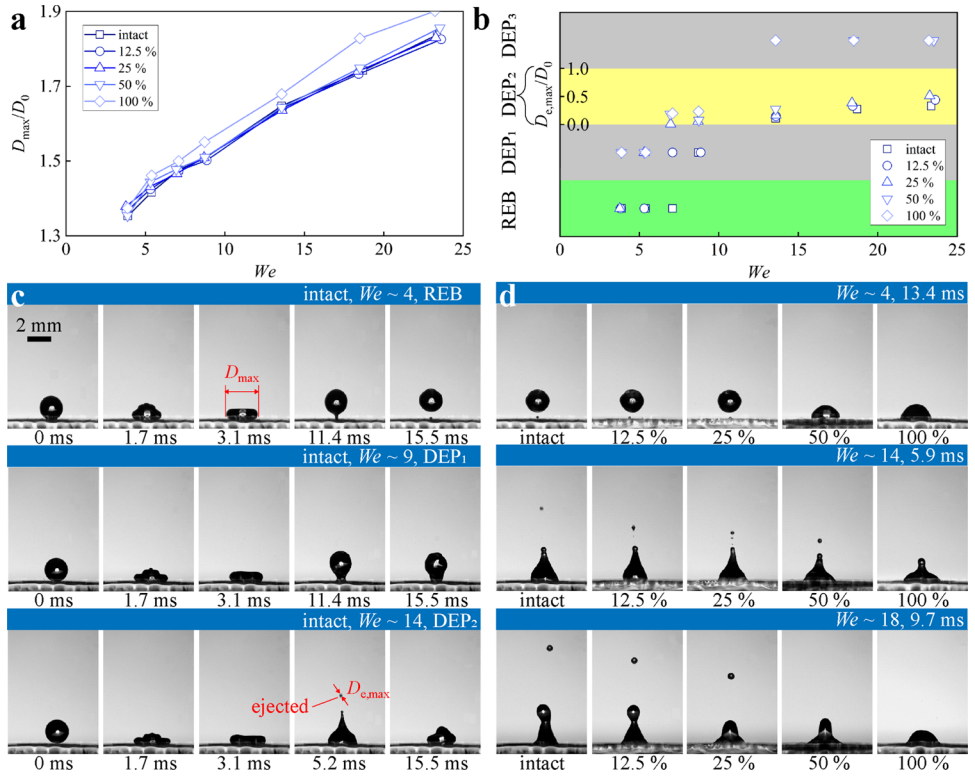

Figure 5. Kinetic water repellency of the self-compensating surface with emulated mechanical damage. (a) Maximum spreading factor D_{max}/D_0 as a function of *We*. (b) After-retracting behaviors including rebounding (REB) and depositing (DEP_1, DEP_2, and DEP_3) as a function of *We*. (c) Snapshots to illustrate different after-retracting behaviors. (d) Snapshots to show the impact of damage degree on after-retracting behaviors.

glass substrates in great consistency with the initial design, thereby indicating our fabrication approach to be an effective avenue to combine the springtail- and plateau-inspired topologies on a single functional surface.

3.3. Water Repellency with Emulated Mechanical Damage. To reveal the self-compensating mechanism of the above artificial surface, in addition to its intact state, we also designed and fabricated another four states to emulate an evolution where mechanical damage was assumed to propagate from high to low due to contact and friction (see Figure 3). Among these four states, the top 12.5 and 25% of mushroom heads first faded away; second, the top 50% of mushroom heads vanished, equaling to a full mushroom-head disappearance on the upper layer; and third, all of the underlying pillars were exposed, indicating a thorough failure of mushroom heads over the whole surface. In comparison to real mechanical damage under a frictional wear, such an emulating approach provides an alternative to exactly control the degree of mechanical deterioration so as to establish the relationship between the damage degree and liquid repellency, thereby quantitatively assessing the self-compensating capacity.

3.3.1. Static Water Repellency. The intact surface exhibited a perfect antipenetrating ability to water droplets (156.4° in Figure 4a) even realized with a hydrophilic photoresist (the contact angle on a smooth plane made of the same photoresist was 67.2°), thus verifying the impressive capacity of a mushroom−pillar combination to transform the initial hydrophilicity into a macroscopic superhydrophobicity. Referring to the well-known Wenzel theory, a roughness will amplify the inherent hydrophilicity as the result of an area extension. The converse effect here was ascribed to not only the mushroom heads[11−19] but also the Fakir effect[35−37] provided by the pillars with a large aspect ratio. Namely, the droplet no longer conformed to the substrate but rested on top of the pillars, while gas pockets were simultaneously trapped underneath the droplet. Gratifyingly, along with the emulated mechanical damage, the surface clearly presented a great self-compensating ability. More precisely, the contact angle retained at 156.5° with 12.5% damage, reduced to 95.0° with 25% damage, and reached 93.2° to approach the hydrophobic−hydrophilic transition with 50% damage. Of note, even when all upper-layer mushroom heads disappeared (50% damage), the repellence still held a hydrophobicity owing to the existence of an intact lower layer that individually undertook the repellent task. The repellency finally reached a hydrophilic value (87.6°) in the circumstance of a complete loss on mushroom heads, thus verifying the Fakir effect of pillars in comparison to the value of 67.2° on a smooth plane. Moreover, the contact angle hysteresis was captured at an unchanged value of 53.1° when the damage percentage increased from 0 to 12.5%. When the damage percentage continued to increase, the droplet got rid of the constraints from the syringe but kept relative rest with the sliding platform, thereby being unable to capture the advancing and receding angles.

For a further assessment of the self-compensating capacity given by a bi-Gaussian stratified arrangement, we established a theoretical model based on the most extant Wenzel and Cassie theories to link the intrinsic contact angle θ and the apparent contact angle θ^* (see Figure 4b, which was clearly modeled in Section S3). As opposed to previous studies, in this model, the material ratio (MR), indicating the probability to find an interfacial element with its height above a specified value, was introduced to define the boundary between the wetted and unwetted regions. In other words, the elements with their pillars

https://dx.doi.org/10.1021/acsami.9b22896
ACS Appl. Mater. Interfaces 2020, 12, 4174−4182

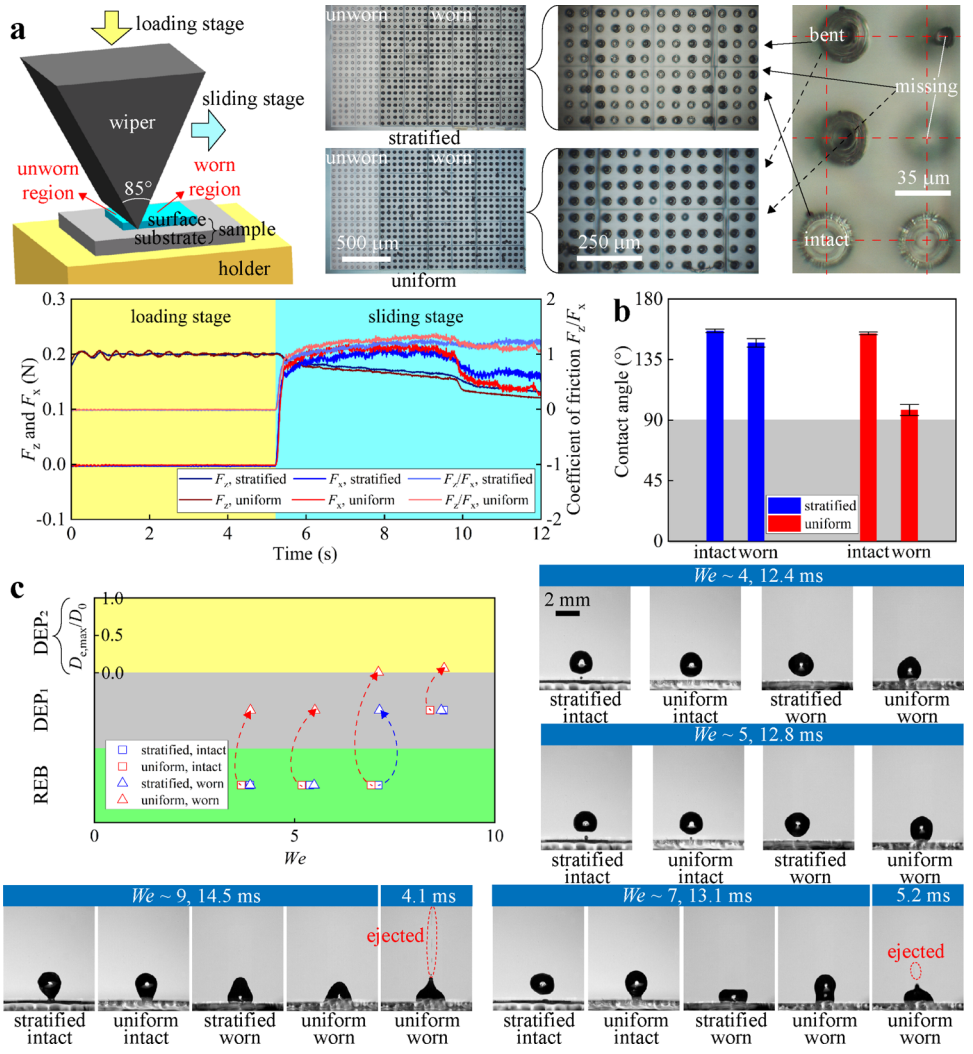

Figure 6. Water repellency of the self-compensating surface with friction-induced mechanical damage. (a) Sliding friction between a rubber wiper and printed surfaces, including the stratified surface and its uniform reference. (b) Contact angles of water droplets. (c) After-retracting behaviors of water droplets as a function of *We*, and corresponding snapshots.

higher than a specified height are wetted, while otherwise are arid (see Figures S3 and S4). Consequently, the macroscopic Wenzel and Cassie states of liquid droplets on a plateau morphology have been divided into four substates. In the W−,W state, the value of MR is 100% with the lower and upper layers both in the Wenzel state; in the W−C state, the MR equals to a value located in the interval of (*Smq*, 100%), with the upper layer in the Wenzel state and the lower layer in the Cassie state; in the W−G state, the MR right equals to *Smq*, indicating the upper layer in the Wenzel state but the lower layer in a gas environment; and in the C−G state, the MR reaches a tiny value in the interval of (0, *Smq*), in which the lower layer stays in the gas environment while the upper layer has entered into the Cassie state. Of course, the value of MR is strongly dependent on the physicochemical attributes of solid and liquid as well as environmental factors, making it a challenge to be theoretically calculated.[25] Anyhow, unlike the previous Wenzel and Cassie models, our model can be used as a crucial probe to estimate the wetting states of the two-component layers, similar to some multiscale wetting models established to distinguish the different wetting states of micro- and nanostructures for hierarchical surfaces.[6,8,38] The measured apparent contact angles in Figure 4a and intrinsic contact angle (67.2° on a smooth plane) were plotted to estimate the values of MR for the self-compensating surface with different mechanical damage (see Figure S5), and are finally summarized in Figure 4c. In the intact or 12.5% damage circumstance, only 7% of structural elements were wetted, indicating the C−G state (note that the *Smq* value of the self-compensating surface was set to 50%, as listed in Table S1); the ratio of wetted elements increased up to 63 and 67% when the damage percentage increased up to 25 and 50%, indicating the W−C state. With a complete loss of mushroom heads, the surface was still located in the W−C state rather than the W−W state because of the Fakir effect of pillars. The unchanged MR when the damage percentage ranged from 0 to 12.5% indicated a great first-level self-compensating ability supported by the upper layer; meanwhile, the MR translated to 63 and 67% when the damage percentage increased to 25 and 50%, thus disclosing the second-level self-compensating capacity ascribed to the uninjured lower layer.

3.3.2. Kinetic Water Repellency. In addition to the static circumstance, the self-compensating capacity of the designed surface should be inspected for kinetic repellency to impinging droplets.[4,7,14,18] We therefore conducted an impacting test to investigate the spreading, retracting, and after-retracting behaviors of water droplets with different impacting velocities

https://dx.doi.org/10.1021/acsami.9b22896
ACS Appl. Mater. Interfaces 2020, 12, 4174−4182

(see Movie S1). Figure 5a presents the maximum spreading factor D_{max}/D_0 as a function of Weber number (We) on the self-compensating surface with emulated mechanical damage. Herein, We, defined as $D_0\rho V_0^2/\sigma$, is a dimensionless pressure index to quantify the ratio between the inertial and capillary forces, where D_0 and V_0 are the diameter and impacting velocity of a droplet in flight before the contact instant, and ρ and σ are the density and surface tension of the droplet. D_{max} is the maximum droplet diameter before the retracting behavior. Up to now, the relationship between D_{max}/D_{max} and We is still a heated subject of controversy because of an open debate on two different scaling laws relying on energy conservation ($D_{max}/D_0 \propto We^{0.5}$) and momentum−mass conservation ($D_{max}/D_0 \propto We^{0.25}$).[39−42] In our study, the latter momentum−mass conservation was preferred (see Figure S6). The intact surface exhibited a greater maximum spreading factor than other damaged cases at the same We, indicating a weakened drag in the spreading phase owing to a mushroom-like topology.

We further investigated the after-retracting behaviors of water droplets and gained a considerable regularity translating from rebounding (REB) to depositing (also from DEP_1, DEP_2 to DEP_3) with an increased We, as summarized in Figure 5b. In the intact state, a rebounding was observed at $We \sim 4$ (visualized in Figure 5c), thus indicating a water resistance to the pressure generated from an impacting event. However, this rebounding motion disappeared when We increased up to ∼9, rendering a depositing response to an impact. When the value of We continued to increase over ∼14, a depositing with the base part pinning onto the surface but the top part ejecting as satellites was observed. We further quantified it by characterizing the maximum diameter of the ejected satellites $D_{e,max}$ and successfully revealed an obvious monotonical increase along with an increased We value.

Figure 5b also shows a considerable regularity of after-retracting behaviors translating from REB, DEP_1, DEP_2 to DEP_3 along with an intensified mechanical damage. At $We \sim 4$ (visualized in Figure 5d), the surface subjected to 12.5 or 25% damage still showed a rebounding response to the dripping droplets, highlighting a great self-compensating ability. However, the after-retracting behavior has switched to a DEP_1 state when the damage percentage reached 50 or 100%. When We increased to ∼7, the surface started to exhibit a DEP_2 behavior with the damage ratio higher than 25%. When We reached ∼14, the surface presented a DEP_2 action in the intact, 12.5, 25, and 50% damage circumstances, where the size of the ejected satellites was proportional to the damage degree. In addition, the dominant role played by the damage degree can also be demonstrated by the DEP_3 phenomenon with 100% damage. In comparison to the fully damaged case, the DEP_3 behavior started to appear with 50% damage when We increased up to ∼18, indicating that a relatively severe damage degree was easier to receive a DEP_3 response. In sum, it can be concluded that a mechanical damage of mushroom heads will weaken the kinetic repellency, thus translating the after-retracting behaviors from REB, DEP_1, DEP_2 to DEP_3. However, our surface can delay this damage-induced translation based on its self-compensating capacity.

3.4. Water Repellency with Real Mechanical Damage.

We applied the self-compensating mechanism drawn from the above-emulated investigation to real mechanical damage caused by frictional wear (see Figure 6a). A triangular rubber wiper was declined to approach a line contact with the underlying printed surface at a specified normal load F_z of 0.2 N, and then was slid over the surface at a speed of 1 mm·s^{-1}. To resolve the impact of a bi-Gaussian stratified arrangement of element heights on our self-compensating surface, we added a uniform reference that fully copied the stratified case, except for uniform element heights. At the sliding stage of the friction test, the interaction of the mated pair (i.e., wiper and printed surface) under the normal load F_z produced a frictional load F_x of around 0.2 N, thereby making the coefficient of friction F_z/F_x around 1, which indicated a starving lubrication (usually implying serious wear). The sliding stage led bending and missing postures to mushroom−pillar elements on the uniform surface, where the missing posture can be classified into mushroom loss and mushroom−pillar coupled loss. However, the stratified surface provided a stark contrast to the uniform one, where low-height elements remained intact due to a stratified arrangement. Of note, a surface under a stratified pattern suggests fewer elements to support the opposite wiper in comparison to a uniform case, highlighting a stricter design rule (e.g., higher element density) required by our self-compensating surface.

Gratifyingly, as depicted in Figure 6b, the contact angle of water droplets on the stratified surface subjected to frictional mechanical damage still remained at 147.4°, as opposed to the uniform case (97.5°), which has dramatically lost its superhydrophobicity to approach a hydrophilic state, thereby validating the self-compensating ability of a bi-Gaussian stratified arrangement in static circumstances. Looking at kinetic circumstances (see Figure 6c extracted from Movie S2), the stratified surface also provided a stark contrast to the uniform one in terms of after-retracting behaviors, indicating that the bi-Gaussian stratified arrangement can offer an unprecedented level of retaining the kinetic repellency regardless of frictional mechanical damage. More precisely, the worn stratified surface retained the original rebounding response at We ∼4 and ∼5, while the uniform surface switched from REB to DEP_1 due to the frictional mechanical damage; as the value of We increased up to ∼7, the original REB behavior transformed into a DEP_1 one on the worn stratified surface but into a DEP_2 one on the worn uniform surface; when We reached ∼9, the worn stratified surface retained the original DEP_1 response, while the uniform surface transformed into a DEP_2 condition from the original DEP_1 state.

4. CONCLUSIONS

In summary, we were inspired by the bi-Gaussian stratified plateaus existing in natural landscapes and engineering industries to design artificial surfaces, which shows much promise in resolving the long-standing issue of improving the interfacial durability of liquid-repelling surfaces using a self-compensating strategy. In such a design, we used the springtail-inspired mushroom topology to decorate a structural configuration to obtain liquid repellency while learning from the plateau-inspired stratified morphology to arrange structural elevation aimed at gaining a self-compensating capacity. 3D direct laser lithography was employed in the micro−nano fabrication to precisely replicate the mushroom configuration following a bi-Gaussian stratified height distribution. Unlike the previous self-supporting and self-healing strategies, on our self-compensating surface, short structural elements will automatically inherit the repelling roles played by taller ones when the latter are damaged by mechanical contact and friction, thereby ensuring stable and sustained liquid repellency. We investigated the self-compensating mechanism of our surface in both static and kinetic circumstances along with emulated mechanical

https://dx.doi.org/10.1021/acsami.9b22896
ACS Appl. Mater. Interfaces 2020, 12, 4174−4182

damage propagating from high to low, finding that the surface, even with a relatively high structural damage (corresponding to 12.5% of the initial structures), exhibited a superstatic repellence with the contact angle above 150° and was able to endure a high pressure arising from impinging droplets. Furthermore, we believe our work to be the first demonstration of a self-compensating strategy under friction-induced mechanical damage, providing an unprecedented level of control over the repellency for a stable and sustained service life. Our study also extended the scope of nature-inspired functional surfaces from conventional biomimetics to geological landscapes.

As an outlook, a detailed parametric discussion is further required to resolve the impact of different bi-Gaussian stratified indexes on optimizing the self-compensating capacity. As the element distance and autocorrelation length have been shown to play crucial roles in liquid repellency, optimizing the spatial characteristics of structural elements can be a potential avenue to drastically elevate the repellence regarding kinetic circumstances with extremely highly impacting events; this would contribute to extending the scope and the use of our self-compensating surfaces. Also, a surface under a stratified pattern usually suggests fewer elements to support the opposite body in comparison to a uniform case, demanding a stricter design rule for the spatial characteristics (e.g., high element density). In addition to the self-compensating inspiration in this study, the particular bi-Gaussian stratified arrangement also offers a flexible choice to tailor interfacial functions when the two layers are designed with different topologies or fabricated with dissimilar materials.

■ ASSOCIATED CONTENT

Supporting Information

The Supporting Information is available free of charge at https://pubs.acs.org/doi/10.1021/acsami.9b22896.

Characterizing and simulating methods of bi-Gaussian stratified morphology; bi-Gaussian stratified indexes to determine element heights; fabrication imperfection; bi-Gaussian stratified wetting model; relationship between maximum spreading factor and Weber number; surface theories; surface design and fabrication; static liquid repellency; kinetic liquid repellency (PDF)

Impacting test with emulated damage (Movie S1) (MP4)

Impacting test with friction-induced damage (Movie S2) (MP4)

■ AUTHOR INFORMATION

Corresponding Authors

Xi Shi − *Shanghai Jiao Tong University, Shanghai, China*; Email: xishi@sjtu.edu.cn

Zhike Peng − *Shanghai Jiao Tong University, Shanghai, China*; Email: z.peng@sjtu.edu.cn

Other Authors

Songtao Hu − *Shanghai Jiao Tong University, Shanghai, China*; orcid.org/0000-0002-8405-3788

Xiaobao Cao − *ETH Zurich, Zurich, Switzerland*

Tom Reddyhoff − *Imperial College London, London, United Kingdom*

Debashis Puhan − *Imperial College London, London, United Kingdom*; orcid.org/0000-0002-7353-8528

Sorin-Cristian Vladescu − *Imperial College London, London, United Kingdom*

Qian Wang − *Imperial College London, London, United Kingdom*

Andrew J. deMello − *ETH Zurich, Zurich, Switzerland*; orcid.org/0000-0003-1943-1356

Daniele Dini − *Imperial College London, London, United Kingdom*; orcid.org/0000-0002-5518-499X

Complete contact information is available at: https://pubs.acs.org/10.1021/acsami.9b22896

Notes

The authors declare no competing financial interest.

■ ACKNOWLEDGMENTS

This work was supported by the China Postdoctoral Science Foundation (2019T120340 and 2017M621458), the National Natural Science Foundation of China (11572192 and 11632011), and the Engineering and Physical Sciences Research Council (EP/N025954/1).

■ REFERENCES

(1) Yao, L.; He, J. Recent Progress in Antireflection and Self-Cleaning Technology - from Surface Engineering to Functional Surfaces. *Prog. Mater. Sci.* **2014**, *61*, 94−143.

(2) Zhan, W.; Yu, S.; Gao, L.; Wang, F.; Fu, X.; Sui, G.; Yang, X. Bioinspired Assembly of Carbon Nanotube into Graphene Aerogel With "Cabbagelike" Hierarchical Porous Structure for Highly Efficient Organic Pollutants Cleanup. *ACS Appl. Mater. Interfaces* **2018**, *10*, 1093−1103.

(3) Han, Z.; Feng, X.; Guo, Z.; Niu, S.; Ren, L. Flourishing Bioinspired Antifogging Materials with Superwettability: Progresses and Challenges. *Adv. Mater.* **2018**, *30*, No. 1704652.

(4) Bird, J. C.; Dhiman, R.; Kwon, H.; Varanasi, K. K. Reducing the Contact Time of a Bouncing Drop. *Nature* **2013**, *503*, 385−388.

(5) Raut, H. K.; Dinachali, S. S.; Loke, Y. C.; Ganesan, R.; Ansah-Antwi, K. K.; Gora, A.; Khoo, E. H.; Ganesh, V. A.; Saifullah, M. S. M.; Ramakrishna, S. Multiscale Ommatidial Arrays with Broadband and Omnidirectional Antireflection and Antifogging Properties by Sacrificial Layer Mediated Nanoimprinting. *ACS Nano* **2015**, *9*, 1305−1314.

(6) Tricinci, O.; Terencio, T.; Mazzolai, B.; Pugno, N. M.; Greco, F.; Mattoli, V. 3D Micropatterned Surface Inspired by Salvinia Molesta via Direct Laser Lithography. *ACS Appl. Mater. Interfaces* **2015**, *7*, 25560−25567.

(7) Sun, Q.; Wang, D.; Li, Y.; Zhang, J.; Ye, S.; Cui, J.; Chen, L.; Wang, Z.; Butt, H.; Vollmer, D.; Deng, X. Surface Charge Printing for Programmed Droplet Transport. *Nat. Mater.* **2019**, *18*, 936−941.

(8) Long, J.; Fan, P.; Gong, D.; Jiang, D.; Zhang, H.; Li, L.; Zhong, M. Superhydrophobic Surfaces Fabricated by Femtosecond Laser with Tunable Water Adhesion: from Lotus Leaf to Rose Petal. *ACS Appl. Mater. Interfaces* **2015**, *7*, 9858−9865.

(9) Koch, K.; Bhushan, B.; Barthlott, W. Diversity of Structure, Morphology and Wetting of Plant Surfaces. *Soft Matter* **2008**, *4*, 1943−1963.

(10) Hensel, R.; Neinhuis, C.; Werner, C. The Springtail Cuticle as a Blueprint for Omniphobic Surfaces. *Chem. Soc. Rev.* **2016**, *45*, 323−341.

(11) Tuteja, A.; Choi, W.; Ma, M.; Mabry, J. M.; Mazzella, S. A.; Rutledge, G. C.; McKinley, G. H.; Cohen, R. E. Designing Superoleophobic Surfaces. *Science* **2007**, *318*, 1618−1622.

(12) Tuteja, A.; Choi, W.; Mabry, J. M.; Mckinley, G. H.; Cohen, R. E. Robust Omniphobic Surfaces. *Proc. Natl. Acad. Sci. U.S.A.* **2008**, *105*, 18200−18205.

(13) Hensel, R.; Helbig, R.; Aland, S.; Braun, H.; Voigt, A.; Neinhuis, C.; Werner, C. Wetting Resistance at Its Topographical Limit: The

Benefit of Mushroom and Serif T Structures. *Langmuir* **2013**, *29*, 1100−1112.
(14) Liu, T.; Kim, C. Turning a Surface Superrepellent even to Completely Wetting Liquids. *Science* **2014**, *346*, 1096−1100.
(15) Hensel, R.; Finn, A.; Helbig, R.; Braun, H.; Neinhuis, C.; Fischer, W.; Werner, C. Biologically Inspired Omniphobic Surfaces by Reverse Imprint Lithography. *Adv. Mater.* **2014**, *26*, 2029−2033.
(16) Kim, J. H.; Shim, T. S.; Kim, S. Lithographic Design of Overhanging Microdisk Arrays Toward Omniphobic Surfaces. *Adv. Mater.* **2016**, *28*, 291−298.
(17) Li, J.; Qin, Q. H.; Shah, A.; Ras, R. H. A.; Tian, X.; Jokinen, V. Oil Droplet Self-Transportation on Oleophobic Surfaces. *Sci. Adv.* **2016**, *2*, No. e1600148.
(18) Yun, G.; Jung, W.; Oh, M. S.; Jang, G. M.; Baek, J.; Kim, N.; Im, S. G.; Jung, H. Springtail-Inspired Superomniphobic Surface with Extreme Pressure Resistance. *Sci. Adv.* **2018**, *4*, No. eaat4978.
(19) Liu, X.; Gu, H.; Wang, M.; Du, X.; Gao, B.; Elbaz, A.; Sun, L.; Liao, J.; Xiao, P.; Gu, Z. 3D Printing of Bioinspired Liquid Superrepellent Structures. *Adv. Mater.* **2018**, *30*, No. 1800103.
(20) Li, Y.; Li, L.; Sun, J. Bioinspired Self-Healing Superhydrophobic Coatings. *Angew. Chem., Int. Ed.* **2010**, *49*, 6129−6133.
(21) Jin, H.; Tian, X.; Ikkala, O.; Ras, R. H. A. Preservation of Superhydrophobic and Superoleophobic Properties upon Wear Damage. *ACS Appl. Mater. Interfaces* **2013**, *5*, 485−488.
(22) Corral, I. B.; Calvet, J. V.; Salcedo, M. C. Use of Roughness Probability Parameters to Quantify the Material Removed in Plateau-Honing. *Int. J. Mach. Tools Manuf.* **2010**, *50*, 621−629.
(23) Hu, S.; Brunetiere, N.; Huang, W.; Liu, X.; Wang, Y. The Bi-Gaussian Theory to Understand Sliding Wear and Friction. *Tribol. Int.* **2017**, *114*, 186−191.
(24) Hu, S.; Reddyhoff, T.; Puhan, D.; Vladescu, S.-C.; Huang, W.; Shi, X.; Dini, D.; Peng, Z. Bi-Gaussian Stratified Wetting Model on Rough Surfaces. *Langmuir* **2019**, *35*, 5967−5974.
(25) Hu, S.; Cao, X.; Reddyhoff, T.; Puhan, D.; Huang, W.; Shi, X.; Peng, Z.; Dini, D. Three-Dimensional Printed Surfaces Inspired by Bi-Gaussian Stratified Plateaus. *ACS Appl. Mater. Interfaces* **2019**, *11*, 20528−20534.
(26) Huovinen, E.; Takkunen, L.; Korpela, T.; Suvanto, M.; Pakkanen, T. T.; Pakkanen, T. A. Mechanically Robust Superhydrophobic Polymer Surfaces Based on Protective Micropillars. *Langmuir* **2014**, *30*, 1435−1443.
(27) Xiao, T. P.; Cifci, O. S.; Bhargava, S.; Chen, H.; Gissibl, T.; Zhou, W.; Giessen, H.; Toussaint, K. C.; Yablonovitch, E.; Braun, P. V. Diffractive Spectral-Splitting Optical Element Designed by Adjoint-Based Electromagnetic Optimization and Fabricated by Femtosecond 3D Direct Laser Writing. *ACS Photonics* **2016**, *3*, 886−894.
(28) Ergin, T.; Stenger, N.; Brenner, P.; Pendry, J. B.; Wegener, M. Three-Dimensional Invisibility Cloak at Optical Wavelengths. *Science* **2010**, *328*, 337−339.
(29) Medina-Sánchez, M.; Schwarz, L.; Meyer, A. K.; Hebenstreit, F.; Schmidt, O. G. Cellular cargo delivery: Toward assisted fertilization by sperm-carrying micromotors. *Nano Lett.* **2016**, *16*, 555−561.
(30) Klein, F.; Richter, B.; Striebel, T.; Franz, C. M.; von Freymann, G.; Wegener, M.; Bastmeyer, M. Two-Component Polymer Scaffolds for Controlled Three-Dimensional Cell Culture. *Adv. Mater.* **2011**, *23*, 1341−1345.
(31) Frenzel, T.; Kadic, M.; Wegener, M. Three-Dimensional Mechanical Metamaterials with a Twist. *Science* **2017**, *358*, 1072−1074.
(32) Hengsbach, S.; Lantada, A. D. Direct Laser Writing of Fractal Surfaces: Strategy to Design and Manufacture Textured Materials. *Adv. Eng. Mater.* **2015**, *17*, 172−180.
(33) Davis, E.; Liu, Y.; Jiang, L.; Lu, Y.; Ndal, S. Wetting Characteristics of 3-Dimensional Nanostructured Fractal Surfaces. *Appl. Surf. Sci.* **2017**, *392*, 929−935.
(34) Lantada, A. D.; Hengsbach, S.; Bade, K. Lotus-On-Chip: Computer-Aided Design and 3D Direct Laser Writing of Bioinspired Surfaces for Controlling the Wettability of Materials and Devices. *Bioinspiration Biomimetics* **2017**, *12*, No. 066004.
(35) Quéré, D. Fakir Droplets. *Nat. Mater.* **2002**, *1*, 14−15.
(36) Quéré, D. Leidenfrost Becomes a Fakir. *Nat. Mater.* **2012**, *11*, 915−916.
(37) Marín, Á. G.; Gelderblom, H.; Susarrey-Arce, A.; van Houselt, A.; Lefferts, L.; Gardeniers, J. G. E.; Lohse, D.; Snoeijer, J. H. Building Microscopic Soccer Balls with Evaporating Colloidal Fakir Drops. *Proc. Natl. Acad. Sci. U.S.A.* **2012**, *109*, 16455−16458.
(38) Verho, T.; Korhonen, J. T.; Sainiemi, L.; Jokinen, V.; Bower, C.; Franze, K.; Franssila, S.; Andrew, P.; Ikkala, O.; Ras, R. H. A. Reversible Switching between Superhydrophobic States on a Hierarchically Structured Surface. *Proc. Natl. Acad. Sci. U.S.A.* **2012**, *109*, 10210−10213.
(39) Tsai, P.; Hendrix, M. H. W.; Dijkstra, R. R. M.; Shui, L.; Lohse, D. Microscopic Structure Influencing Macroscopic Splash at High Weber Number. *Soft Matter* **2011**, *7*, 11325−11333.
(40) Kim, H.; Lee, C.; Kim, M. H.; Kim, J. Drop Impact Characteristics and Structure Effects of Hydrophobic Surfaces with Micro- and/or Nanoscaled Structures. *Langmuir* **2012**, *28*, 11250−11257.
(41) Laan, N.; de Bruin, K. G.; Bartolo, D.; Josserand, C.; Bonn, D. Maximum Diameter of Impacting Liquid Droplets. *Phys. Rev. Appl.* **2014**, *2*, No. 044018.
(42) Kim, H.; Park, U.; Lee, C.; Kim, H.; Kim, M. H.; Kim, J. Drop Splashing on a Rough Surface: How Surface Morphology Affects Splashing Threshold. *Appl. Phys. Lett.* **2014**, *104*, No. 161608.

https://dx.doi.org/10.1021/acsami.9b22896
ACS Appl. Mater. Interfaces 2020, 12, 4174−4182